Supporting Information

Movie S1. The fiber-shaped aqueous lithium ion batteries were drilled through during powering light emission diodes**.**

Experimental Section

Materials. P-chlorophenol, 1, 4, 5, 8-naphthalenetetracarboxylic dianhydride, ethylene diamine and Li_2SO_4 were ordered from Sinopharm Chemical Reagent Co., Ltd. They were used as received. Heat-shrinkable tube was provided by Suzhou Dasheng Materials Tech Co. Ltd.

Preparation of carbon nanotube fibers. Spinnable carbon nanotube (CNT) arrays were synthesized via chemical vapor deposition at 740 ^{o}C for 10 min with Fe (1.5 nm)/Al_2O_3 (5 nm) on a silica wafer as catalyst. For the catalyst, Fe and Al_2O_3 were deposited on silica wafer via electron-beam evaporation at rates of 0.5 and 2 Å/s, respectively. Ethylene was used as the carbon precursor with a flowing rate of 90 sccm. Hydrogen (30 sccm) and argon (400 sccm) were mixed as the carrier gas. The highly aligned CNT sheets were continuously drawn out of the spinnable CNT array. The aligned CNT fiber was prepared by scrolling ten layers of CNT sheets.

Characterization. The structure were characterized via field emission scanning electron microscopy (SEM, S-4800, Hitachi Inc., Japan) and Fourier transform infrared spectrometer (FT-IR, IRPrestige-21, Shimadz Inc., Japan). Three-electrode cells were used to test the electrochemical properties of fiber electrodes. Either polyimide (PI)/CNT fiber or $LiMn_2O_4$ (LMO)/CNT fiber was employed as a working electrode. Excessive activated carbon and saturated calomel electrode were used as counter and reference electrodes, respectively. All the electrochemical measurements were performed on Arbin electrochemical station (MSTAT-5V/10Ma/16Ch). The weight of the CNT fiber, PI/CNT and LMO/CNT hybrid fiber were measured by a microbalance (Sartarious SE2, resolution of 0.1 μg).

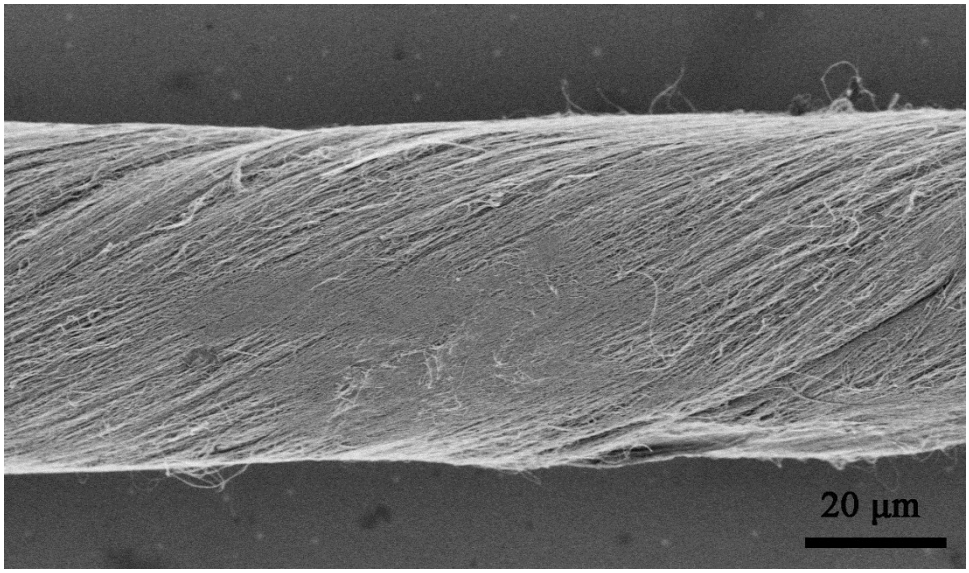

Figure S1. Scanning electron microscopy (SEM) image of a CNT fiber at a low magnification.

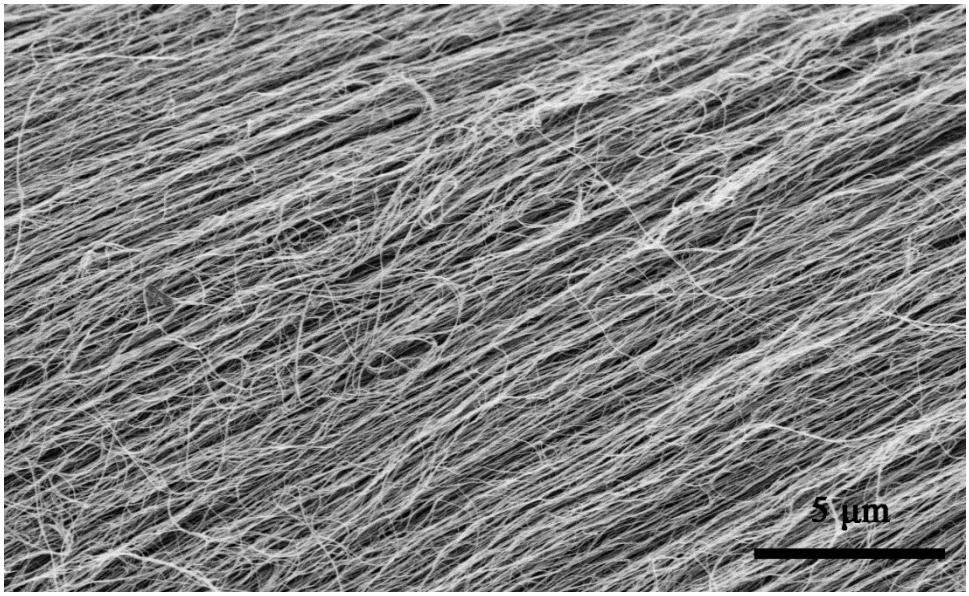

Figure S2. SEM image of a CNT fiber at a high magnification.

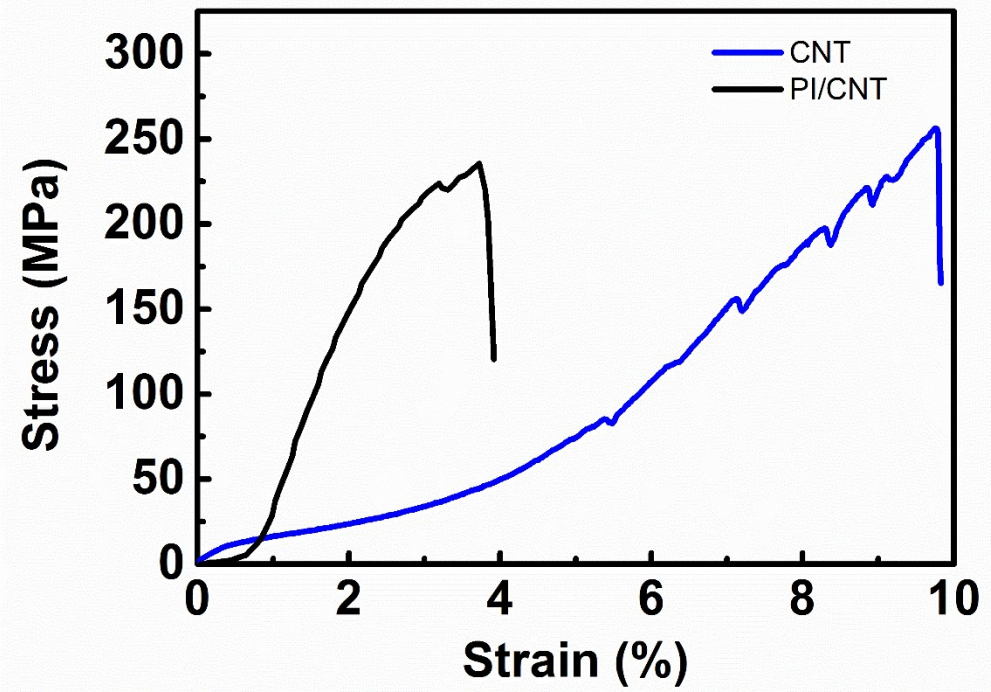

Figure S3. Stress-strain curves of the pure CNT and PI/CNT hybrid fibers.

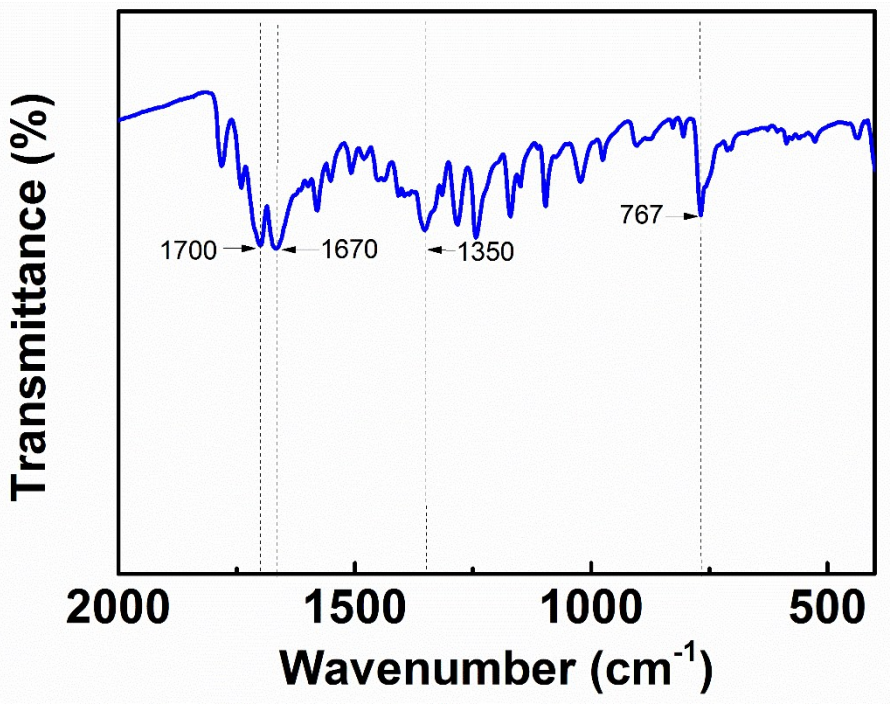

Figure S4. Fourier transform infrared spectroscopy spectrum of PI/CNT hybrid fiber.

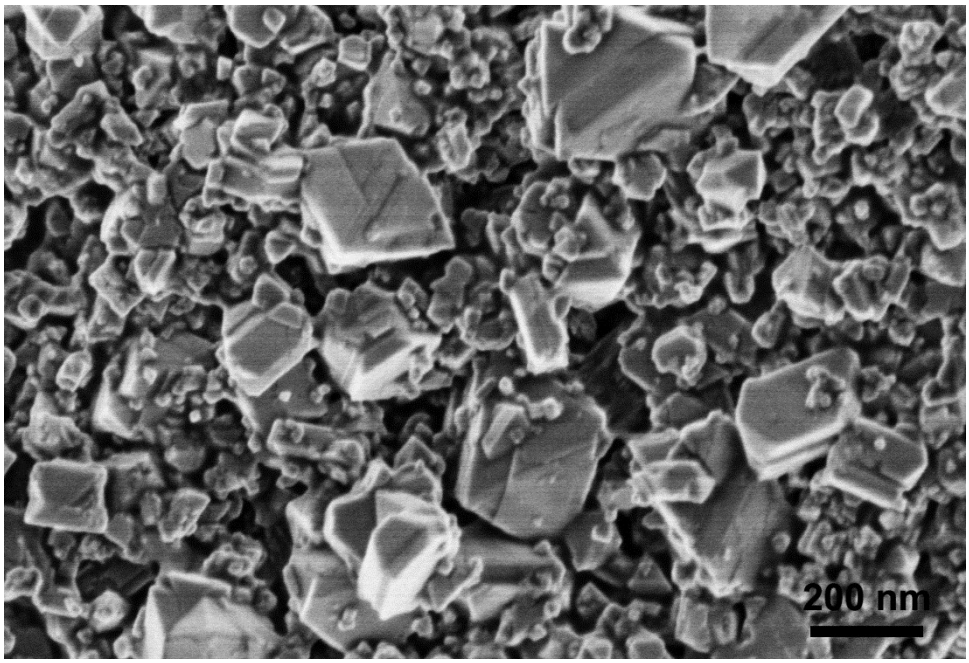

Figure S5. SEM image of LMO nanoparticles.

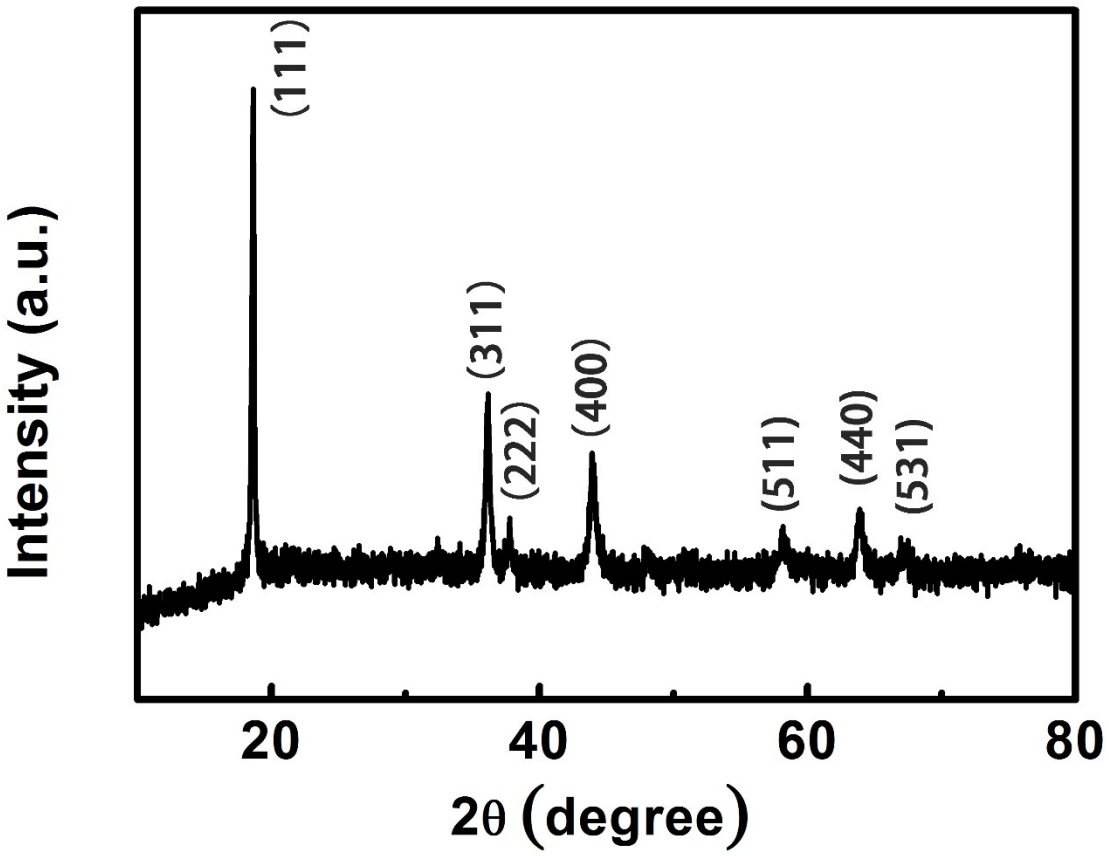

Figure S6. X-ray diffraction pattern of LMO.

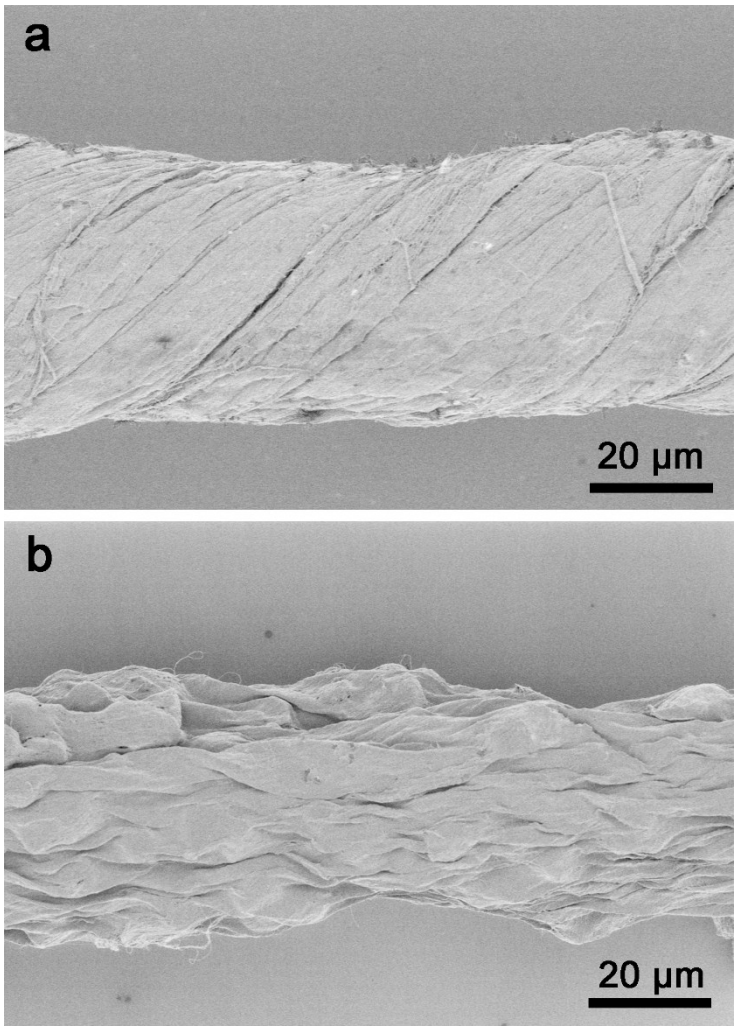

Figure S7. (a) and (b) SEM images of PI/CNT and LMO/CNT hybrid fibers after bending for 1000 cycles, respectively.

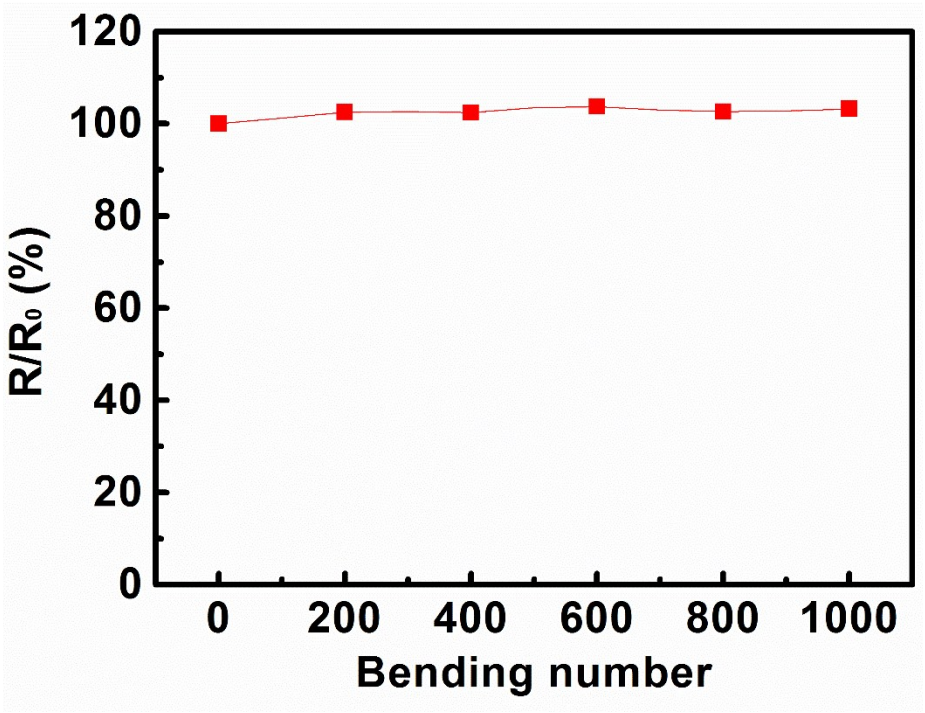

Figure S8. Dependence of electrical resistance of PI/CNT hybrid fiber on bending number. R_0 and R correspond to electrical resistances before and after bending, respectively.

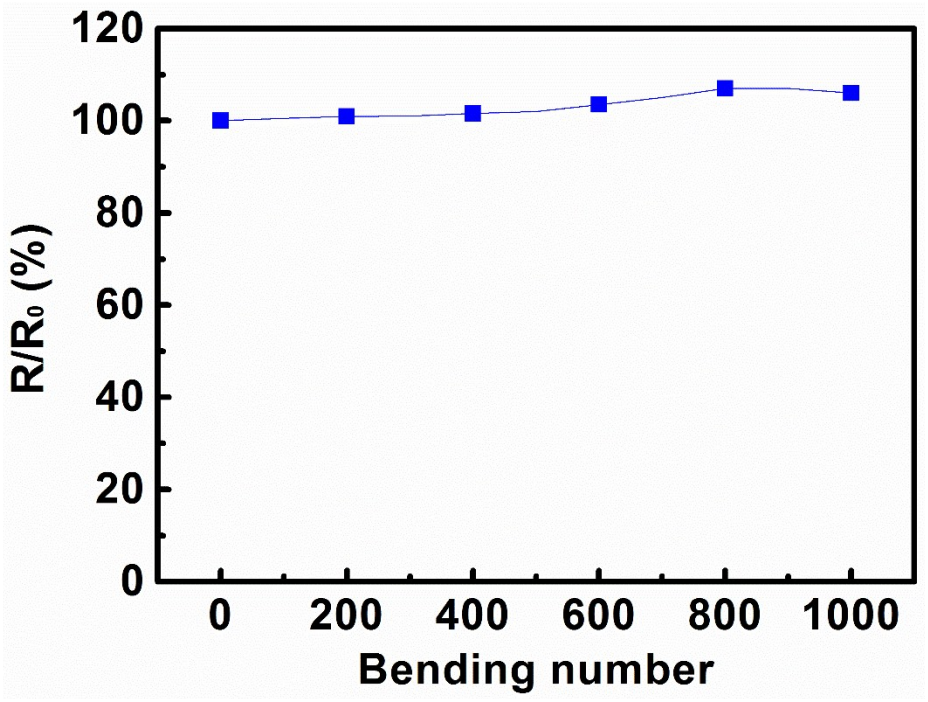

Figure S9. Dependence of electrical resistance of LMO/CNT hybrid fiber on bending number. R_0 and R correspond to electrical resistances before and after bending, respectively.

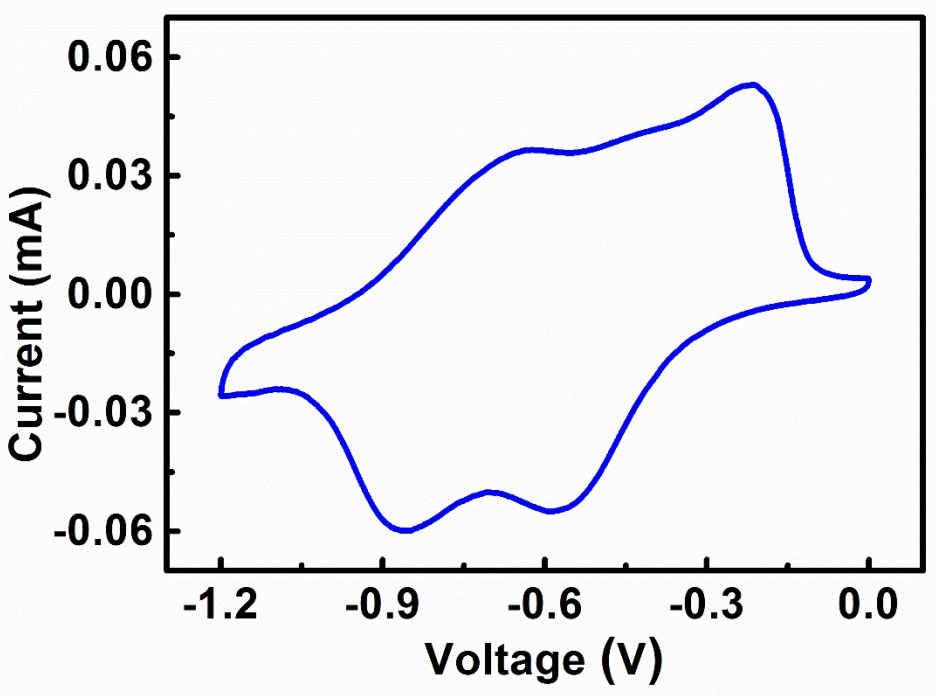

Figure S10. Cyclic voltammogram of PI/CNT hybrid fiber at a scan rate of 5 mV/s in a voltage window of -1.2-0 V versus saturated calomel electrode.

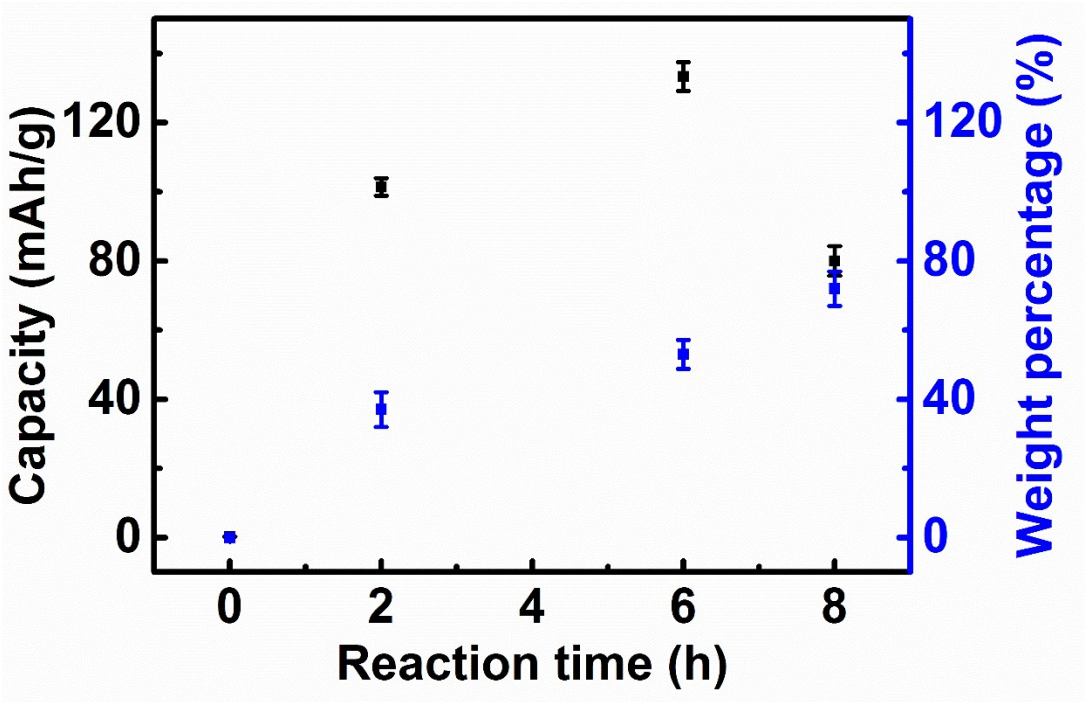

Figure S11. Dependence of specific capacity of PI/CNT hybrid fiber and the weight percentage of PI on reaction time.

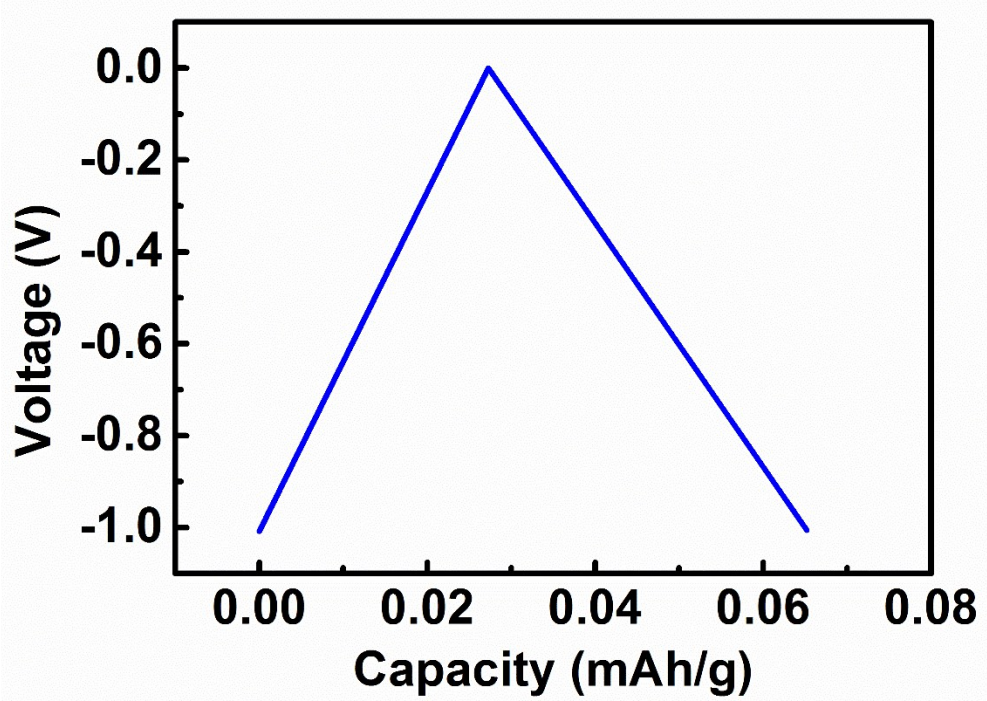

Figure S12. Charge-discharge curve of a bare CNT fiber

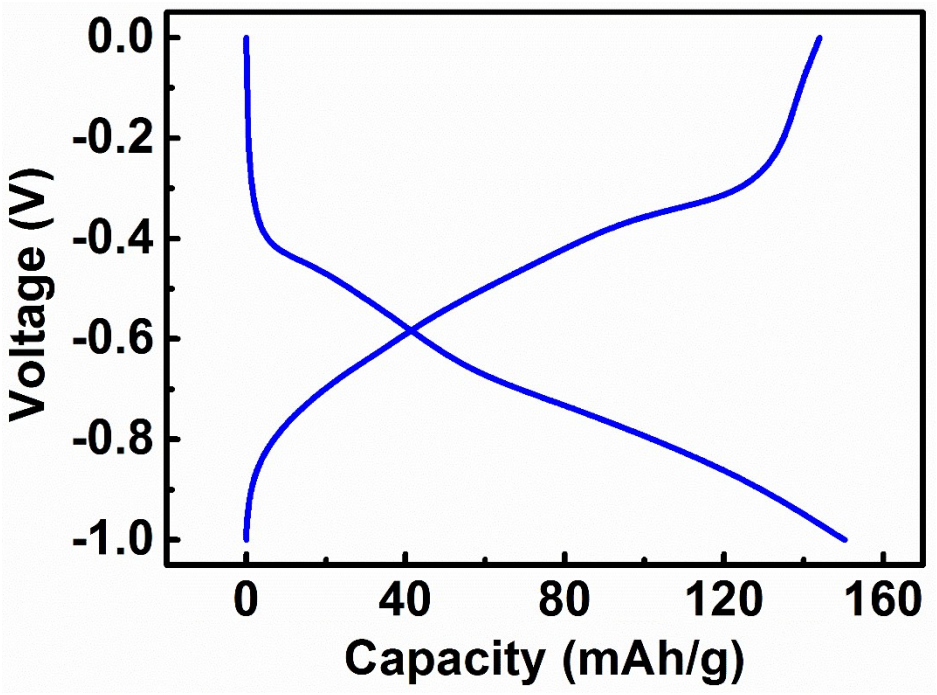

Figure S13. Charge and discharge curves of the PI/CNT fiber electrode at a current rate of 1C (1C=183 mA/g).

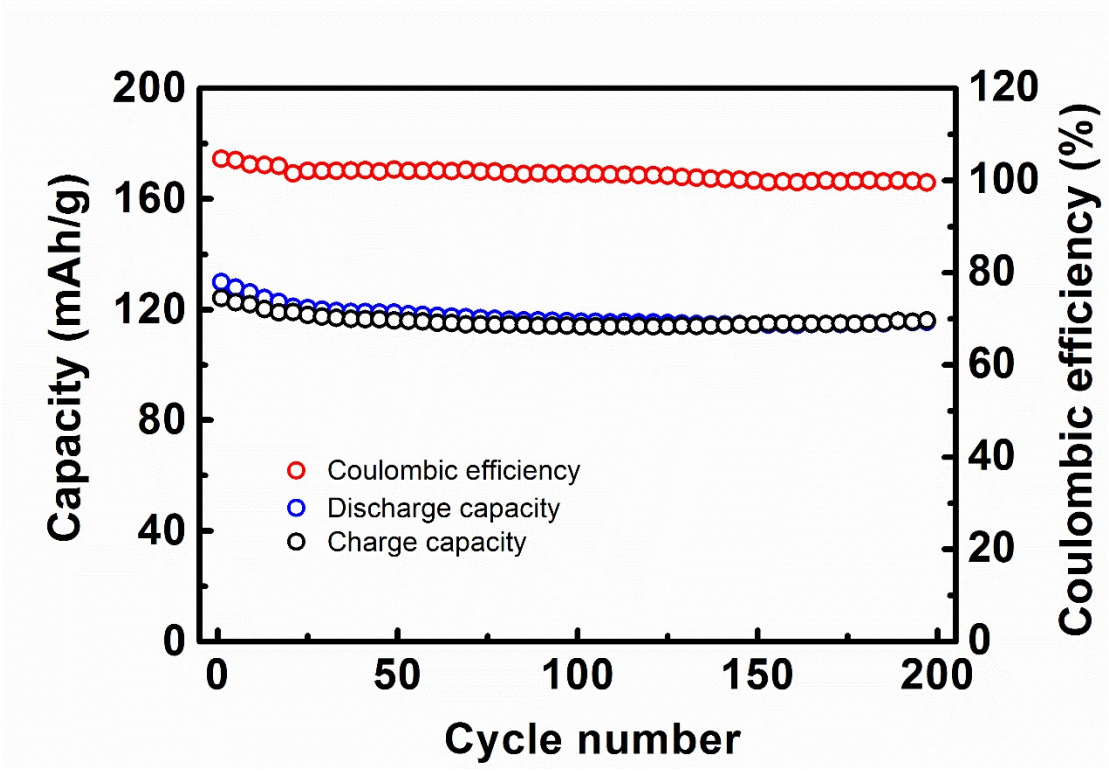

Figure S14. Cycling stability test of the PI/CNT hybrid fiber electrode at a current rate of 20 C.

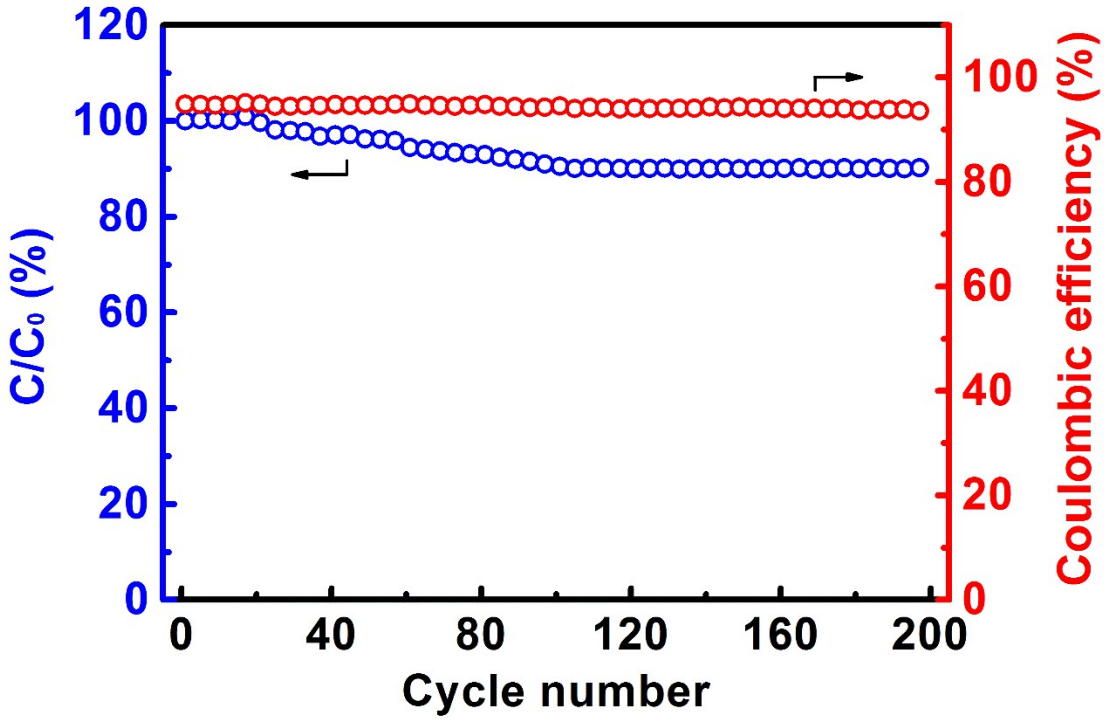

Figure S15. Cycling stability test of the LMO/CNT hybrid fiber electrode at a current rate of 10 C.

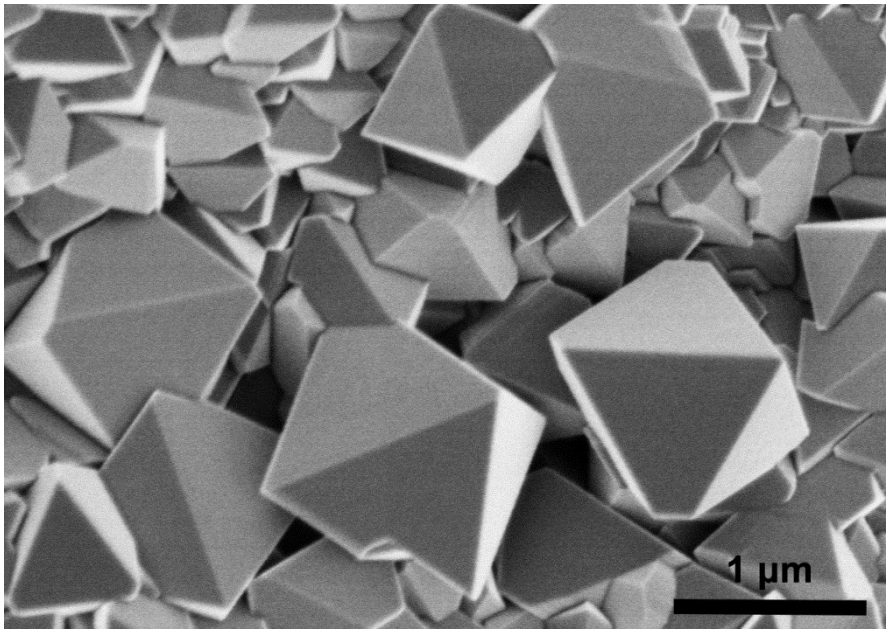

Figure S16. SEM image of the commercial LMO particles.

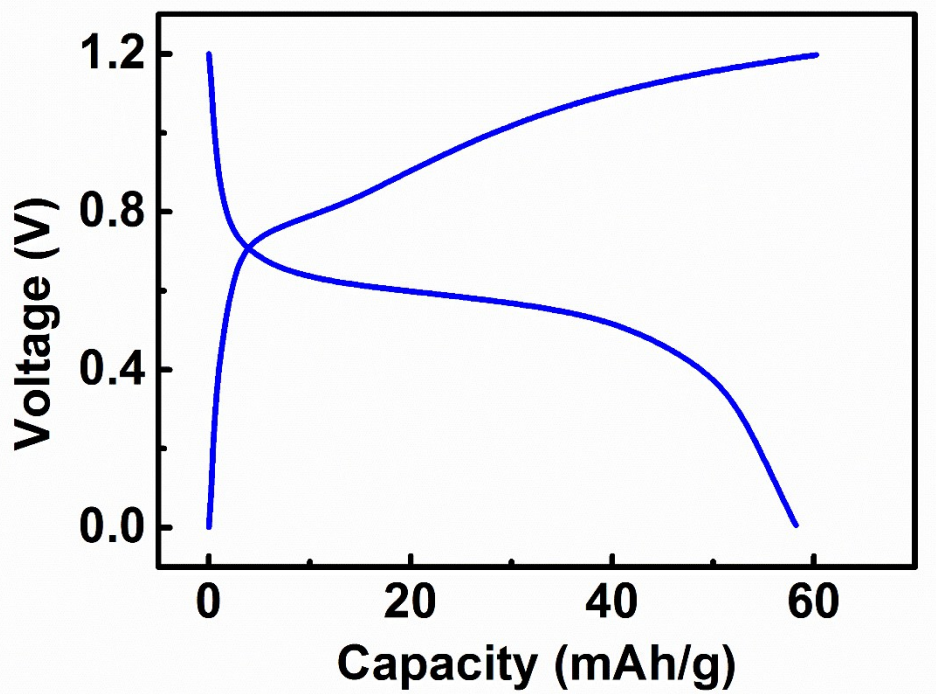

Figure S17. Charge and discharge curves of the commercial LMO at a current rate of 20 C (1C=148 mA/g).

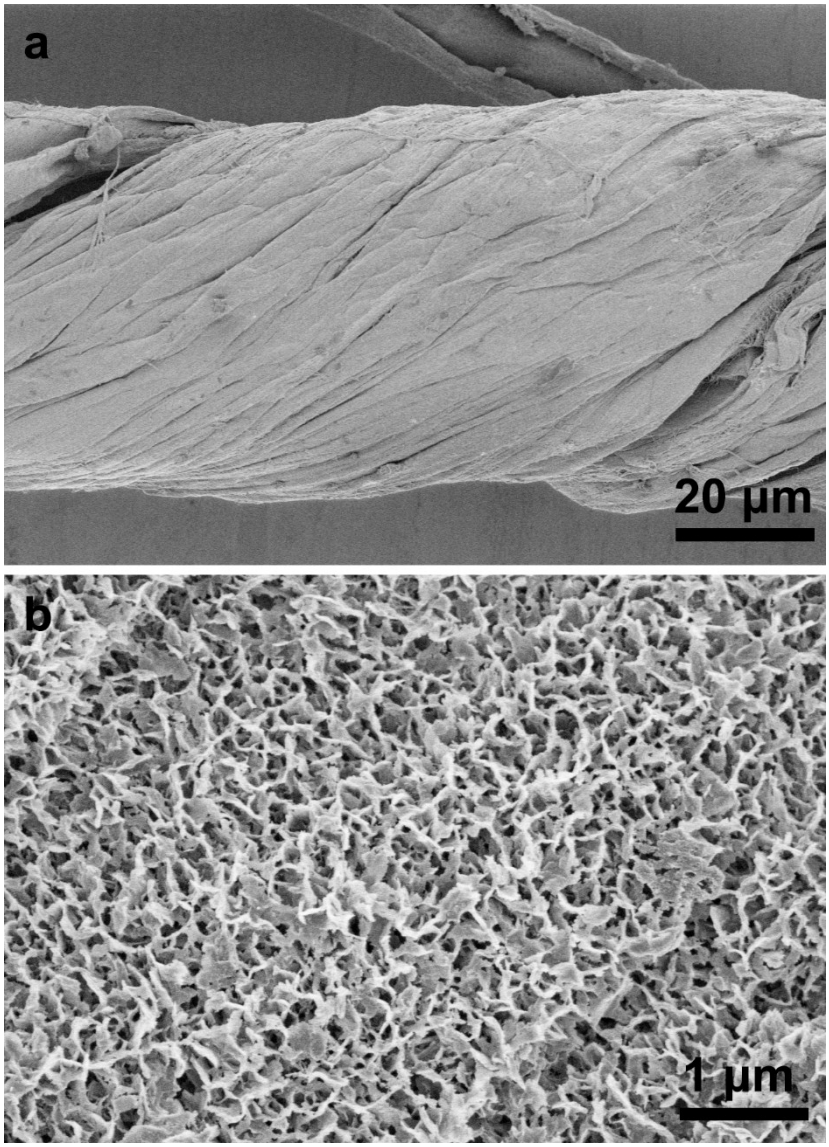

Figure S18. (a) and (b) SEM images of PI/CNT hybrid fiber after charging and discharging for 50 cycles at low and high magnifications, respectively.

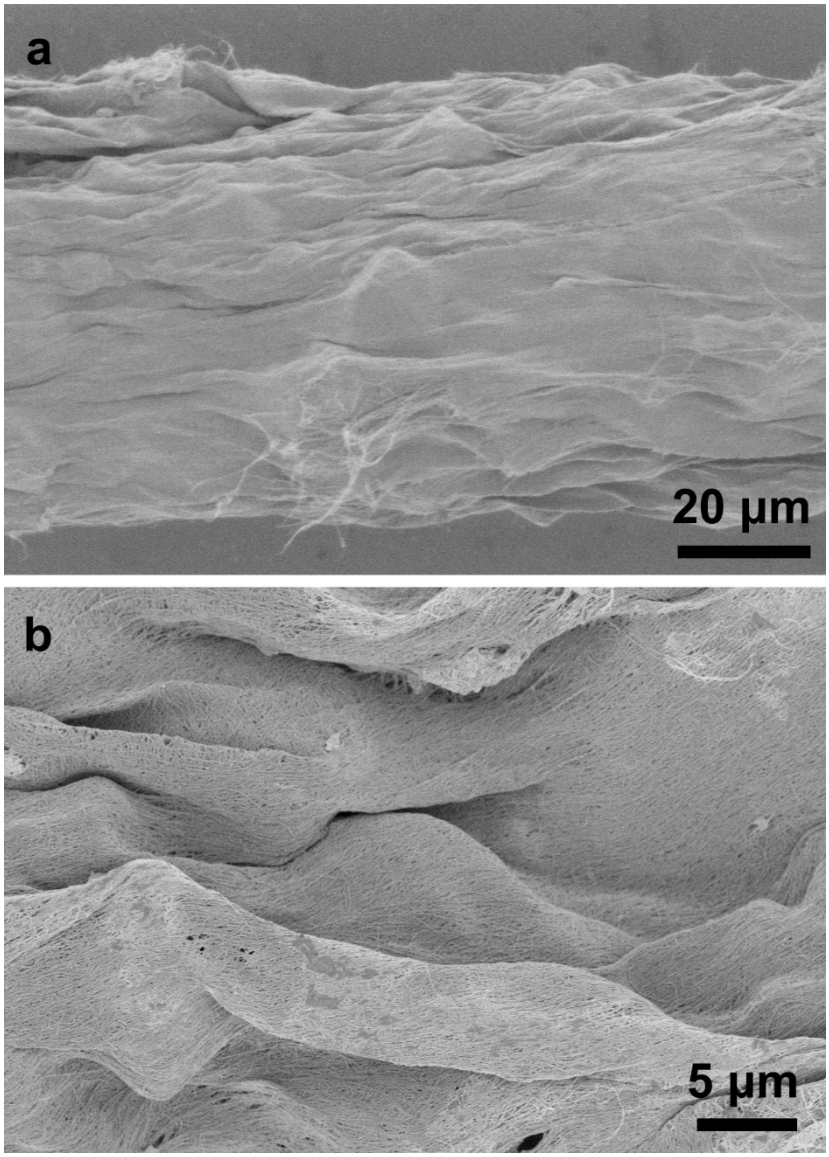

Figure S19. (a) and (b) SEM images of LMO/CNT hybrid fiber after charging and discharging for 50 cycles at low and high magnifications, respectively.

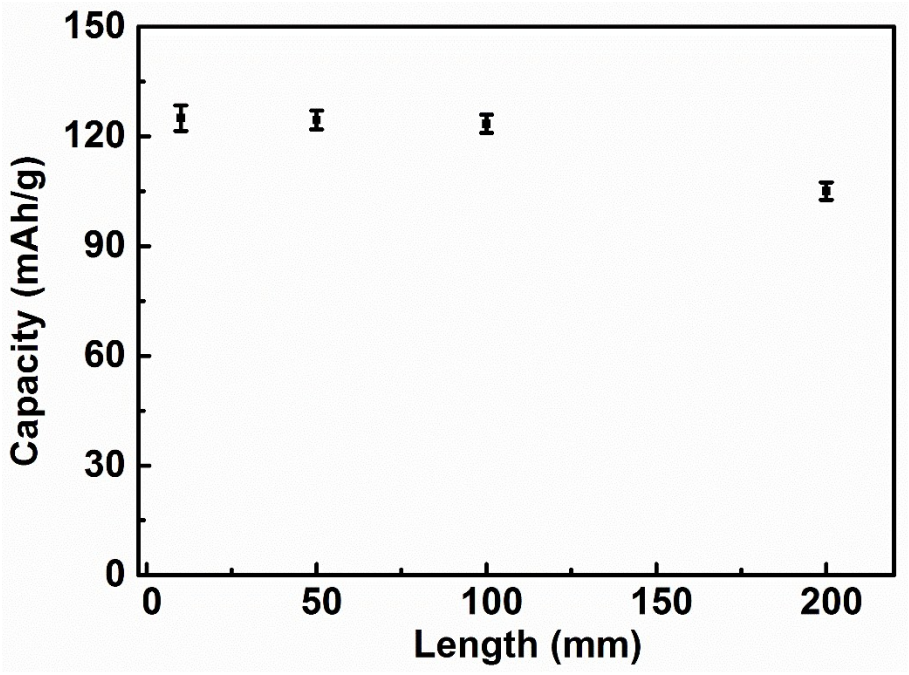

Figure S20. Dependence of specific capacity on the length of the fiber-shaped aqueous lithium ion batteries.

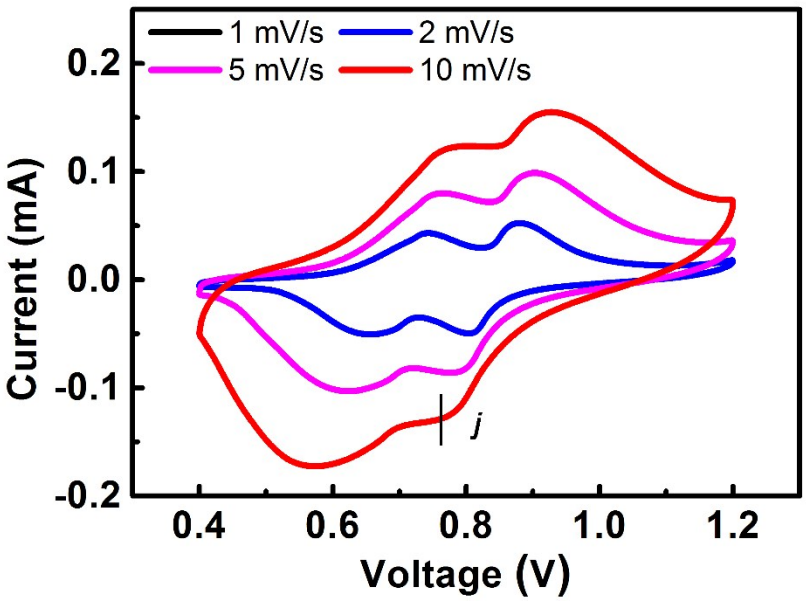

Figure S21. Cyclic voltammogram of an LMO/CNT fiber electrode at increasing scan rates from 1 to 10 mV/s.

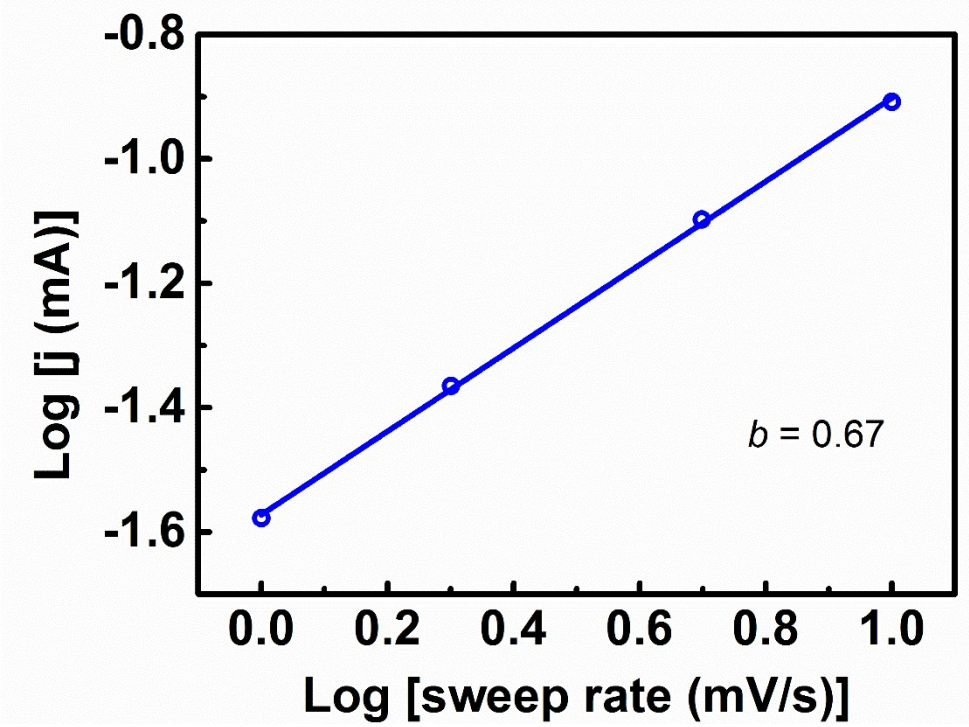

Figure S22. Determination of the *b* value according to the relationship between sweep rate (mV/s) and current (mA) of the LMO/CNT fiber electrode.

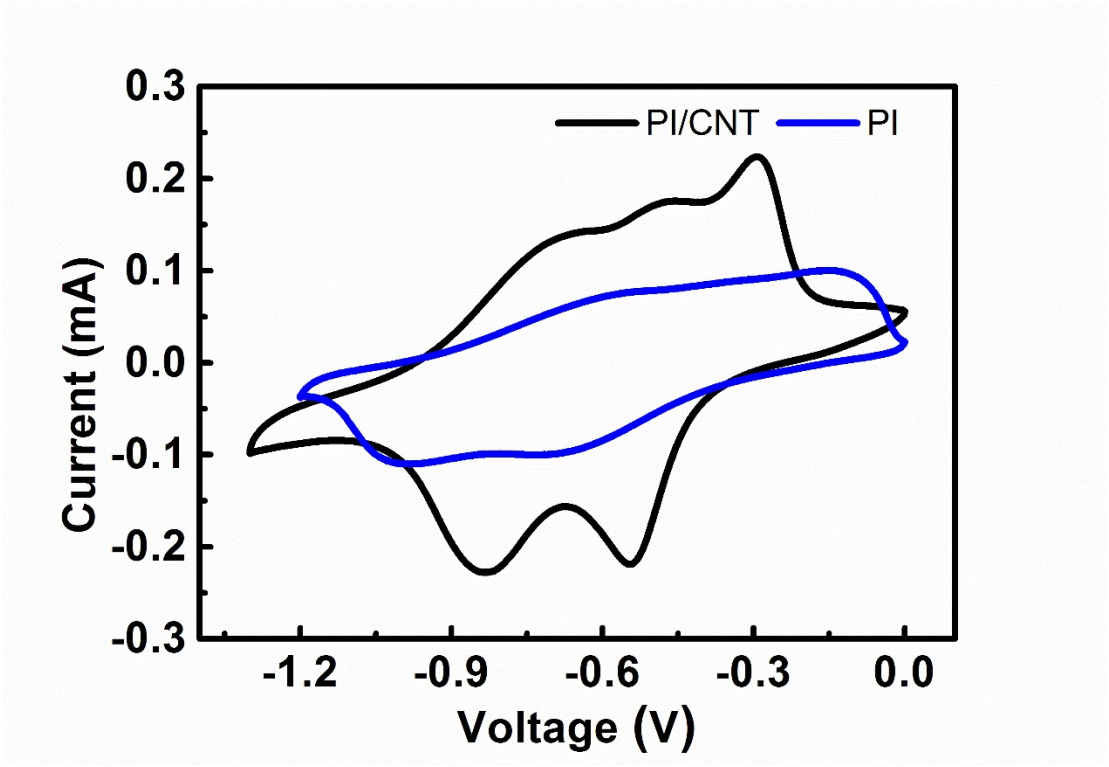

Figure S23. Cyclic voltammograms of PI/CNT and PI electrodes at a scan rate of 1 mV/s.

Table S1. Comparison of the PI/CNT anode with the representative anode in aqueous lithium ion batteries.

ref	Materials	Capacity(mAh/g)/ Current rate		Retention (%) (no. of cycles)
This work	PI/CNT	144/1 C	86/600 C	92 (200)
S1	VO_2	160.8/0.8 C	-	51 (50)
S2	$LiTi_2(PO_4)_3$	103/1 C	89/10 C	97 (120)
S3	C-TiP_2O_7	91/0.1 C	10/5 C	91 (150)
S4	MoO_3/PPy	60/1 A g^{-1}	-	90 (150)
S5	$LiTi_2(PO_4)_3$	113/0.2 C	110/1 C	89 (100)

Table S2. Comparison of our fiber-shaped aqueous lithium ion batteries with the representative fiber-shaped energy storage devices and planar aqueous lithium ion batteries (LIB, lithium ion battery; SC, supercapacitor; the energy and power densities being specified to the weight or volume of electrodes)

ref	System	Electrolyte	Structure	Average voltage (V)	Capacity (mAh/g)	Retention (%) (no. of cycles)	Enenrgy density (Wh/kg)	Enenrgy density (mWh/cm^3)	Power density (W/kg)	Power density (W/cm^3)
This work	PI/LMO LIB	Aqueous	Flexible fiber-shaped	1.4	123	96 (1000)	48.93	14.3	10217.7	2.98
S6	$Li_4Ti_5O_{12}$/LMO LIB	Organic	Flexible fiber-shaped	2.2	138	85 (100)	27	-	880	-
S7	Si/LMO LIB	Organic	Flexible fiber-shaped	3.2	106.5	87 (100)	242	-	480	-
S8	CNT-graphene SC	Aqueous	Flexible fiber-shaped	0.5	-	93 (10000)	-	6.3	-	1.085
S9	RGO-CNT SC	Aqueous	Flexible fiber-shaped	0.4	-	94 (2000)		3.5	-	1.0
S10	$NiCo_2O_4$ SC	Aqueous	Flexible fiber-shaped	0.5	-	78 (5000)	-	1.44	-	17
S11	CNT-RGO SC	Aqueous	Flexible fiber-shaped	0.5	-	96 (10000)	-	2.4	-	0.3
S12	$NiCo_2O_4$- PPy SC	Aqueous	Flexible fiber-shaped	0.15	-	90 (5000)	17.5	-	4000	-
S13	Carbon fiber-polyaniline/ Carbon fiber SC	Aqueous	Flexible fiber-shaped	0.8	-	81 (10000)	-	2	-	10.22
S14	$LiTi_2(PO_4)_3$/LMO LIB	Aqueous	Rigid planar	1.5	80	80 (200)	60		800	
S4	MoO_3-PPy /LMO LIB	Aqueous	Rigid planar	1.22	90	82 (150)	45		6000	
S15	V_2O_3 LIB	Aqueous	Rigid planar	0.7	131	88 (50)	-	-	-	-
S16	TiP_2O_7/LMO LIB	Aqueous	Rigid planar	1.2	90	33 (100)	60	-	2000	-

Reference

S1 F. Wang, Y. Liu, C. Liu, *Electrochim. Acta,* 2010, **55**, 2662.

S2 Z. Liu, X. Qin, H. Xu, G. Chen, *J. Power Sources,* 2015, **293**, 562.

S3 W. Wu, S. Shanbhag, A. Wise, J. Chang, A. Rutt, J. F. Whitacre, *J. Electrochem. Soc.,* 2015, **162**, A1921.

S4 W. Tang, L. Liu, Y. Zhu, H. Sun, Y. Wu, K. Zhu, *Energy Environ. Sci.,* 2012, **5**, 6909.

S5 C. Wessells, F. La Mantia, H. Deshazer, R. A. Huggins, Y. Cui, *J. Electrochem. Soc.,* 2011, **158**, A352.

S6 J. Ren, Y. Zhang, W. Bai, X. Chen, Z. Zhang, X. Fang, W. Weng, Y. Wang, H. Peng, *Angew. Chem. Int. Ed.,* 2014, **126**, 7998.

S7 W. Weng, Q. Sun, Y. Zhang, H. Lin, J. Ren, X. Lu, M. Wang, H. Peng, *Nano Lett.,* 2014, **14**, 3432.

S8 D. Yu, K. Goh, H. Wang, L. Wei, W. Jiang, Q. Zhang, L. Dai, Y. Chen, *Nat. Nanotechnol.,* 2014, **9**, 555.

S9 L. Kou, T. Huang, B. Zheng, Y. Han, X. Zhao, K. Gopalsamy, H. Sun, C. Gao, *Nature Commun.,* 2014, **5**, 3754.

S10 Q. Wang, X. Wang, J. Xu, X. Ouyang, X. Hou, D. Chen, R. Wang, G. Shen, *Nano Energy,* 2014, **8**, 44.

S11 B. Wang, X. Fang, H. Sun, S. He, J. Ren, Y. Zhang, H. Peng, *Adv. Mater.,* 2015, **27**, 7854.

S12 W. Xiong, X. Hu, X. Wu, Y. Zeng, B. Wang, G. He, Z. Zhu, *J. Mater. Chem. A,* 2015, **3**, 17209.

S13 H. Jin, L. Zhou, C. L. Mak, H. Huang, W. M. Tang, H. L. W. Chan, *Nano Energy,* 2015, **11**, 662.

S14 J. Y. Luo, Y. Y. Xia, *Adv. Funct. Mater.,* 2007, **17**, 3877.

S15 Y. Sun, S. Jiang, W. Bi, C. Wu, Y. Xie, *J. Power Sources,* 2011, **196**, 8644.

S16 K. Sun, D. A. Juarez, H. Huang, E. Jung, S. J. Dillon, *J. Power Sources,* 2014, **248**, 582.